INORGANIC CHEMISTRY
FRONTIERS

RESEARCH ARTICLE

View Article Online
View Journal | View Issue

Cite this: *Inorg. Chem. Front.*, 2023, **10**, 2484

Exploring the potential as molecular quantum-dot cellular automata of a mixed-valence Ru2 complex deposited on a Au(111) surface

Nicolás Montenegro-Pohlhammer, [a] Carlos M. Palomino[b] and Carmen J. Calzado *[b]

A key requirement for the implementation of molecular quantum dot cellular automata (mQCA) is the ordered attachment of molecules on surfaces. In this work we explore by means of state-of-the art quantum chemistry calculations different aspects of the deposition of a mixed-valence **Ru2$^+$** complex on Au(111), underlined as a promising component in mQCA. Our results provide information about the geometry adopted by the **Ru2$^+$** molecule and the counterion PF_6^- on the metal surface and the electronic structure of the doublet ground state, with the excess charge localized on one side of the molecule, not only on the Ru centre, but also involving a part of the 12-carbon bridging chain, which could explain the pair of bright/dim features of STM images. Our calculations also test the functionality as the mQCA of the **Ru2$^+$** molecule, evaluating the response curve under an applied electric field as perturbation, and the electronic distribution of two neighbouring **Ru2$^+$** molecules forming a four-dot cell, with a diagonal organization of the two excess charges. To the best of our knowledge, this is the first study devoted to the analysis of the electronic structure and mQCA functionality of deposited mixed-valence molecules.

Received 11th December 2022,
Accepted 21st March 2023

DOI: 10.1039/d2qi02647c

rsc.li/frontiers-inorganic

1. Introduction

The concept of quantum-dot cellular automata (QCA) was introduced by von Neumann and Ulam in the 1940s[1] and experimentally demonstrated by Lent and coworkers in 1993,[2] as a possible alternative to current electronics.[3] A QCA cell consists of either four quantum dots positioned at the corners of a square or two dots (half-cell) arranged side by side or head to tail. A quantum dot is a region in the cell where charge can localize. In the case of the four-dot QCA, there are two extra electrons (or holes) which can move among the dots. These two charges are favourable for adopting a diagonal arrangement due to Coulomb repulsion, resulting in two degenerate states that can be used to encode logic "0" and "1" states (Fig. 1). In the two-dot QCA, an extra electron (hole) can be localized in one of the two sites. The central idea is that the Coulomb interaction between neighbouring cells is sufficient to transmit the binary signal with no current flow and low power dissipation. Then, QCA devices are expected to achieve a relevant saving of energy and a significant increase in processing speed.

QCA has been experimentally demonstrated using metal islands of about 60 nm as dots but only at very low temperature (100 mK).[4,5] To improve the operation temperature and reduce the size of QCA devices, it has been suggested there is a possibility of replacing the dots by a single molecule with two or more redox active centres, known as molecular QCA (mQCA).[6–9] The candidate molecule needs to have bistable charge configurations that can be switched by Coulomb interactions. Several candidate systems have been proposed, including organic and organometallic mixed-valence (MV) complexes, zwitterionic boron–allyl complexes, metal cluster carboxylates, and double-cage fluorinated fullerene anions.[10–23] Together with the experimental characterization, much effort has been devoted to the development of theoretical models[24–29] aimed to establish the parameters controlling their functionality, such as the intracell Coulomb interaction, the electron transfer integral and the vibronic coupling.

Mixed-valence molecules are by far the most studied. Let us consider a complex with two redox sites, with one excess electron that can move between them. When this electron is localized on one of the redox sites, *e.g.*, the left side, the molecule represents a "1" bit. The electron transfer to the right site changes the ground state configuration, and the molecule represents now a "0" bit. A moderate coupling between the redox sites is required to obtain a rapid exchange of the charge between them. This requirement can be fulfilled by a class II

[a]*Laboratory of Theoretical Chemistry, Faculty of Chemistry and Biology, University of Santiago de Chile (USACH), 9170022 Santiago, Chile*
[b]*Departamento de Química Física, Universidad de Sevilla, c/ Prof. García González, s/n 41012, Sevilla, Spain. E-mail: calzado@us.es*

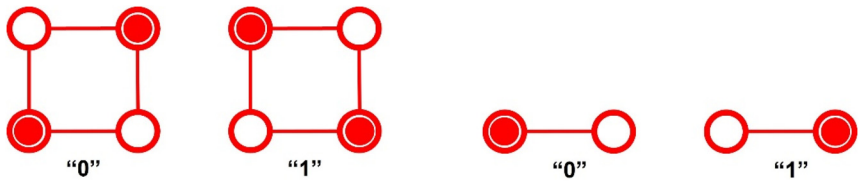

Fig. 1 Schematic four-dot QCA (left) and two-dot half-QCA (right). Coulomb repulsion keeps the electrons (in red) at diametrical sites. Binary information "0" or "1" is encoded in the charge distribution.

MV complex in Robin–Day classification. Additionally, the operation as mQCA requires the molecules to be attached to a substrate in ordered arrays, which in some cases implies functionalization with specific anchor ligands.[13,18–20,30]

Recently, Guo and Kandel[31] investigated by means of scanning tunneling microscopy (STM) the deposition of the dinuclear complex *trans*-[Cl(dppe)$_2$Ru(C≡C)$_6$Ru(dppe)$_2$Cl] **Ru2** on a Au(111) surface (dppe = diphenylphosphinoethane) and its potential as a two-charge-container QCA cell. The dinuclear complex consists of two Ru-centred phenylphosphine groups connected by a linear 12-carbon chain (Fig. 2). The STM images indicated that the **Ru2** molecules formed monolayers of ordered stripes on Au(111) at low temperature, where the molecules lined up side-by-side into rows. The mixed valence **Ru2**$^+$ complex was obtained by mixing **Ru2** once deposited on the gold surface with ferrocenium hexafluorophosphate, [Fe(η^5-C$_5$H$_5$)$_2$][PF$_6$]. The oxidation to **Ru2**$^+$ introduced an additional positive charge on the complex that can tunnel between the two metal-centred groups. The oxidized **Ru2**$^+$ molecules maintained the organization in stripes, but the two dots appeared to have different contrasts in STM images. This has been related to the localization of the extra charge in one of the two metal-centred redox sites. The STM images showed also additional small features assigned to the PF_6^- anions, which compensated the extra charge of **Ru2**$^+$.

It is the aim of this work to explore by means of state-of-the-art quantum chemistry calculations the deposition of the **Ru2**$^+$ complex on Au(111) and those features that highlight its potential as mQCA. We have optimized the molecule on the gold surface in the presence of the counterion by means of periodic density functional calculations. Once optimized, we analyzed the low-lying states of the oxidized **Ru2**$^+$ molecule by wave-function based approaches and found that the active redox sites do involve not only the metal centres but also part of the 12-carbon wire. The PF_6^- anion on the surface is placed close to one of the metal centres, compensating the extra charge of the oxidized **Ru2**$^+$ cation, in line with the experimental STM images.

Finally the functional suitability of **Ru2**$^+$ as mQCA cells was investigated by simulating the impact of an external electric field on the charge distribution of the molecule with the geometry adopted on the Au(111) surface, and by simulating the electronic behavior of two paired molecules, which showed the expected antipodal charge configuration.

These results confirm the stability of the **Ru2**$^+$ molecule deposited on the metal substrate, the charge localization in the effective dots, the antiparallel alignment of the charge on neighboring molecules on the surface and the capability of switching upon application of an electric field.

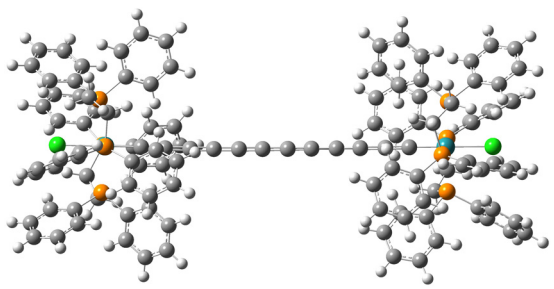

Fig. 2 Representation of the **Ru2** molecule: dark green, grey, white, orange and light green correspond to Ru, C, H, P and Cl, respectively.

2. Description of the models and computational details

Since there are no available X-ray data for the **Ru2** system – in fact difficulties in obtaining crystals suitable for structure determination have been mentioned in the literature[32–34] – we have used the X-ray crystallographic data of a similar dinuclear Ru(II) complex[33] *trans*-[(L)(dppe)$_2$Ru(C≡C)$_6$Ru(dppe)$_2$(L)][PF$_6$]$_2$, with L = N≡CCH$_2$CH$_2$NH$_2$ to build the computational models. The terminal N≡CCH$_2$CH$_2$NH$_2$ ligands were replaced by chlorine atoms,[33] with a Ru–Cl distance of 2.4 Å, as in many other Ru–Cl bonds.[35] These bond distances were optimized in the subsequent calculations.

We have optimized first the isolated molecule in the mixed-valence states, using a modified B3LYP exchange–correlation functional, $E_{XC} = (1 - a)(E_X^{LSDA} + \Delta E_X^{B88}) + aE_X^{HF} + E_C^{LYP}$, with 35% of exact exchange (a = 0.35) and LYP correlation.[36] This functional has been suggested as a practical protocol to deal with mixed-valence systems in a set of benchmark studies.[37,38] Additionally, the molecule has been optimized with the rPBE functional to compare with the results obtained from periodic calculations, where the modified B3LYP functional is not available. The ORCA code[39] has been employed to run the optimizations, with the basis sets of quality def2SVP for all atoms.

Once optimized, the molecule was deposited on the Au (111) surface, represented by a three-layer slab, with a total of

336 Au atoms. This model of the surface based on a three-layer slab has been extensively used in studies dealing with the deposition of molecules on metal surfaces.[40–45] Both the molecule and the upper layer of the gold slab were optimized with the rPBE functional and basis set of DZP quality for all atoms, except Au atoms represented by SZP basis, using periodic conditions with the SIESTA code.[46] The mesh cut-off energy was set to 300 Rydberg for both the real and reciprocal space grids in all calculations, with a self-consistency tolerance for the convergence of the energy and the density matrix of 1.0×10^{-4} eV.

Next, we performed CASSCF calculations on the optimized geometry of the isolated molecule and the molecule deposited on the metal surface to extract information on the nature and energy of its low-lying states and the extension of the electronic localization of the redox sites. The basis sets of quality def2SVP were employed for all the atoms. State-average CASSCF (7/4) calculations for the four lowest doublet roots were carried out with the ORCA code.[39] The active space contains seven electrons, distributed on the Ru $4d_{xz}$ and $4d_{xy}$ orbitals combined with the π_z and π_y orbitals of the carbon bridging chain.

Finally, we analyse the functionality as the QCA of the deposited **Ru2**$^+$ molecule. First, we simulated the response curve of the complex under an external electric field, with the aim of testing the functional suitability of **Ru2**$^+$ as QCA cells. State-average CASSCF(7/4) calculations of the two-lowest quasi-degenerated doublet states are performed in the presence of an external electric field oriented along the long axis of the molecule (field in the x axis, almost parallel to the intramolecular Ru–Ru axis) with increasing strength. The spin density on each effective redox site is evaluated from Mulliken spin population analysis. The uniform electric field is generated by the TITAN code,[47] as a set of point charges distributed in two circular plates separated by 90 Å on opposite sides of the molecule. Each plate contains 33 circular rings, separated by 2.8 Å, where the point charges are homogeneously distributed.

Additionally, we calculated the electronic structure of the cell composed of two **Ru2**$^+$ molecules, parallel to each other, with the Ru centres at the vertices of a rhombus, following the packing observed in the STM images of the **Ru2**$^+$[PF_6^-] monolayer on Au(111).[31] In this case, state average CASSCF calculations of the four lowest triplet roots are performed, with active spaces containing 14 electrons in 8 active orbitals.

3. Results and discussion

3.1. Isolated Ru2$^+$ molecules

The optimization of the isolated **Ru2**$^+$ molecule with the modified B3LYP functional provides a quite symmetric structure, with only small differences between both Ru centres. A similar structure results from the optimization with the rPBE functional (Fig. 3). The 12-carbon wire presents a linear configuration with alternating short/long bonds. The C–C distances are *ca.* 1.283 Å/1.324 Å, which could be compared with the distances in the homovalent molecule, 1.270 Å/1.342 Å, obtained at the same level of calculation. Hence, the oxidation reduces the bond length alternation on the π-conjugated linker. This trend has been experimentally observed on one-electron oxi-

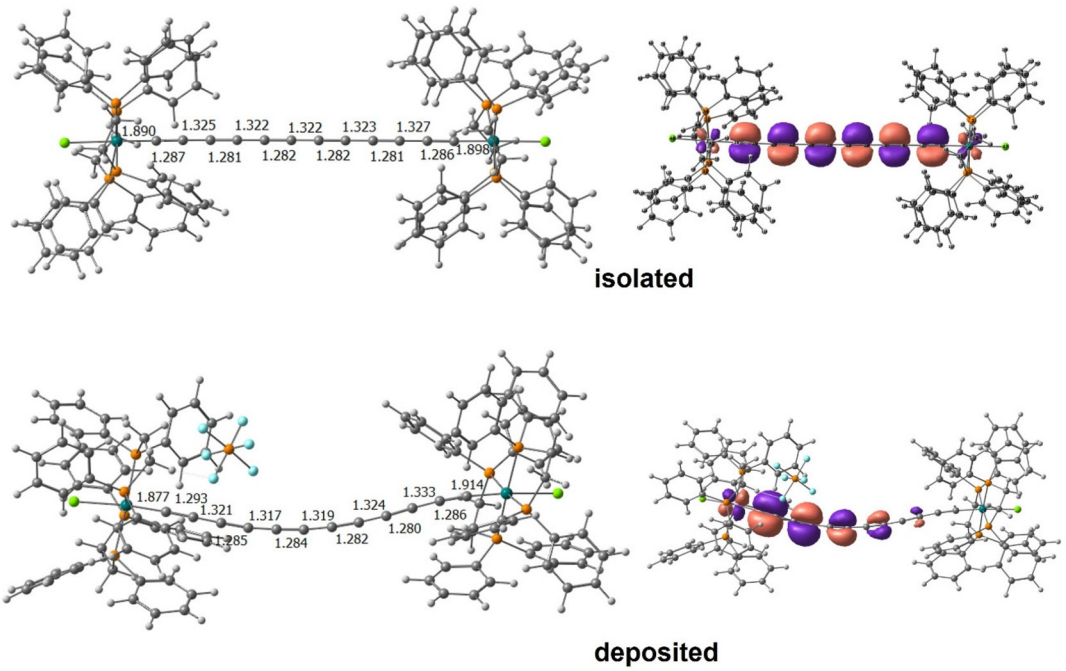

Fig. 3 (left) C–C and C–Ru bond distances in the **Ru2**$^+$ molecule from rPBE calculations on the optimized geometries for the isolated (top) and deposited molecule on Au(111) in the presence of the PF_6^- counterion (bottom). (right) Singly occupied orbitals of the lowest doublet state from state average CASSCF(7/4) calculations.

dized dinuclear metal M complexes with all-carbon –(C≡C)$_2$– as a linker, with M = Fe, Mo, Re and Ru as the metal centre.[48] The terminal carbon atoms of the bridge occupy the axial positions of the Ru coordination spheres, with Ru–C distances of 1.918 Å and 1.925 Å for Ru(1) and Ru(2), respectively (1.891 Å and 1.898 Å for the rPBE functional). The carbon wire is symmetrically aligned with the x axis, with its π orbitals placed on the xz (π_z) and xy (π_y) planes.

At this level of calculation, the singly occupied molecular orbital (SOMO) is completely delocalized, resulting from the antibonding combination of the Ru 4d$_{xy}$ orbitals with the highest occupied π_y orbital of the carbon chain (Fig. 4, top). The SOMO is close in energy to a doubly occupied orbital corresponding to an equivalent combination involving the Ru 4d$_{xz}$ orbitals and the occupied π_z orbital of the carbon chain (HOMO−1 in Fig. 4). The nature of the SOMO indicates that the unpaired electron is highly delocalized between both metal centres with a significant participation of the carbon chain. The partial oxidation of the bridge is in line with the decrease of the bond length alternation observed for the optimized geometry of the **Ru2**$^+$ molecule. This behaviour has been previously found in mixed-valence diruthenium compounds with polyynediyl linkers, where the radical centre tends to localize on the π-conjugated bridge.[48,49] In fact, a three state model has been suggested to analyse the behaviour of these MV complexes,[50] an extension to the general Marcus–Hush two-state model, involving additionally a bridge-localized state.

A similar description is obtained at the CASSCF level, and the lowest doublet is represented by a single configuration, where the singly occupied orbital presents the same shape as the SOMO from the B3LYP* (or rPBE) calculation (Fig. 3), *i.e.*, the unpaired electron occupies a molecular orbital resulting from the antibonding combination of the HOMO of the polyynediyl-bridge and the 4d$_{xy}$ Ru orbitals. The first-excited doublet state is separated by 399 cm^{-1} to the ground state. The wavefunction of this excited state is dominated by a configuration where the singly occupied orbital involves the Ru 4d$_{xz}$ orbitals and the occupied π_z orbitals, in consonance with the nature of the HOMO−1 of the DFT description.

Therefore, independent of the approach, the isolated **Ru2**$^+$ molecule presents a marked charge delocalization and could then be classified as a class III Robin–Day mixed-valence compound. Hence, using concepts of the Marcus–Hush electron transfer theory[51–56] for the isolated **Ru2**$^+$ molecule, the resonance energy ($2|J|$, with J being the electronic coupling between the diabatic states) is larger than the reorganization energy (λ), $2|J|/\lambda > 1$, and the ground state potential-energy surface shows a single minimum.

3.2. Deposited Ru2$^+$ molecules on Au(111)

The complex is now deposited on the Au(111) surface and optimized in the presence of the PF_6^- anion with periodic rPBE calculations. Different conformations have been tested for both the molecule and the counterion, and the most stable one is shown in Fig. 5. The z axis corresponds to the normal to the surface. The molecule lies flat, with its long axis (x) parallel to the surface. The molecule on the surface is arranged in such a way that the intramolecular metal–metal axis forms an angle of ~8° with respect to the [1$\bar{1}$0] direction.

The molecule presents distortions both in the carbon chain, now slightly bent toward the surface although with similar C–C distances to those in the isolated molecule

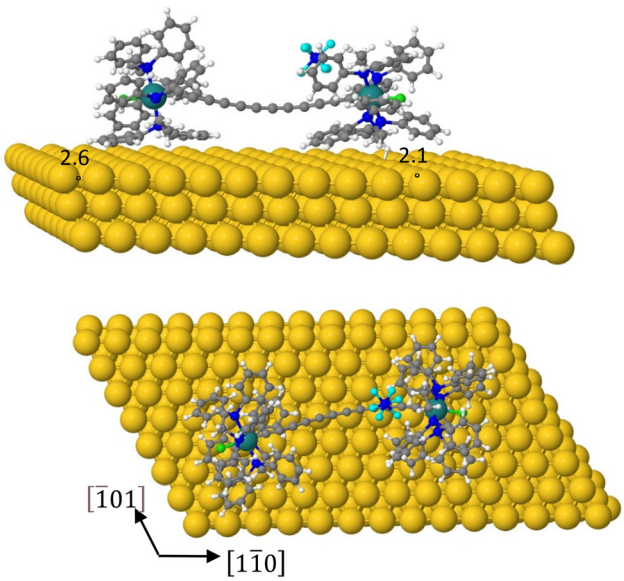

Fig. 5 Top and side views of the **Ru2**$^+$ molecule and PF_6^- ions deposited on the Au(111) surface. Au, Ru, C, F, Cl, P and H are represented by yellow, green, grey, cyan, light green, blue and white balls, respectively.

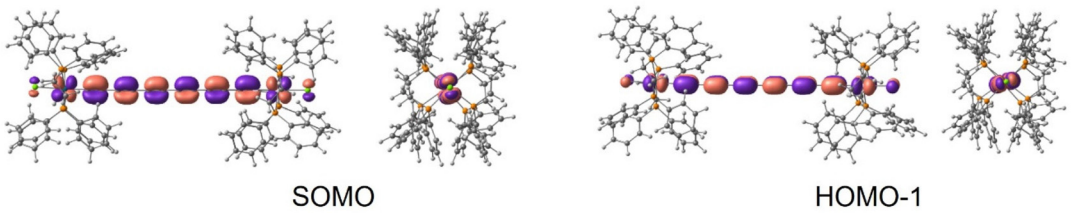

Fig. 4 Front and side views of the (left) SOMO and (right) HOMO−1 for the isolated **Ru2**$^+$ molecule at the B3LYP* level, similar for the rPBE description.

(Fig. 3), and the phenyl groups close to the metal surface, which adopt a quasi-planar orientation with respect to the surface, favoring the contacts with the Au atoms (with C···Au distances of about 2.6 Å). The PF_6^- group is close to one of the two Ru centres, slightly shifted with respect to the carbon chain, in line with the description resulting from the interpretation of the STM images.[31] The Ru–C distances are 1.877 Å and 1.914 Å, and the shortest one corresponds to the metal Ru (1) close to the PF_6^- group. These Ru–C bond distances can be compared with those in the isolated molecule (1.891 Å and 1.898 Å at the same level of calculation). Hence the deposition differentiates the two metal centres, which display dissimilar metal–C bond distances, in contrast to those of the isolated molecule. Both the orientation with respect to the surface and the presence of the counterion next to one end group of **Ru2**$^+$ are in agreement with the description based on the STM images of the **Ru2**$^+$[PF_6^-] monolayer on Au(111).[31]

With the optimized geometry of the deposited molecule, we performed a new set of state-averaged CASSCF(7/4) calculations of the four lowest doublet roots. The ground state is described by a single configuration, the singly occupied orbital being localized in a part of the molecule, close to the PF_6^- ion, distributed on Ru(1) and the closest six carbon atoms of the C_{12} wire. The participation of the carbon atoms decreases as the distance to Ru(1) increases (Fig. 3). The first excited doublet state, as in the case of the isolated molecule, is close in energy (474 cm^{-1} above the ground state), showing a similar localization of the unpaired electron on a side of the molecule. In the second and third excited doublet states, the hole is localized on the opposite side of the molecule, around Ru(2), and the energy difference with the ground state gives an estimate of the reorganization energy of the deposited molecule in the presence of the counterion ($\lambda \sim 1.97$ eV). It is important to note that this value can be affected by different factors such as the quality of the basis sets, nature and size of the active space and number of averaged roots in the CASSCF approach. It should be considered just as a rough estimate of λ. We can then describe **Ru2**$^+$ once deposited on the gold surface as a class II mixed-valence compound, where the mobile hole localizes in an effective redox site, involving Ru(1) and the closest six carbon atoms of the 12-carbon chain. Hence, the Ru(2) end side group has a formal charge of +2*e* while the Ru(1) effective site has a charge of +3*e*, carrying the hole (or the unpaired electron). The PF_6^- counterion is placed next to Ru(1) optimizing the electrostatic interactions. Then, both the deposition and the presence of the counterion drive the localization of the charge in this system. In other words, the deposition and the presence of the counterion enhance the reorganization energy, being finally larger than the resonance energy ($2|J|/\lambda < 1$), giving rise to a double-welled potential-energy surface and the localization of the charge.[51–56] As previously suggested,[33,57] a mixed-valence compound classified as class III in solution or the gas-phase (here, isolated) should not be excluded as a potential candidate of mQCA, since the perturbation introduced by the interaction with the substrate, the counterion or the applied voltage could induce the charge localization, as is the case for the **Ru2**$^+$ complex on Au(111). Note that the localization of the extra charge on the redox sites is just one of the requirements. In fact, the key factor for mQCA operation is that the polarization of the molecule can be switched by the action of the field induced by the neighbouring polarized driver cell.

3.3. Functionality as mQCA

Finally, we analyse the potential of this system for mQCA operation. A key requirement is that the molecular charge distribution can be switched by the coulombic perturbation produced by a neighbouring molecule switching from one state to another. The Coulomb field produced by the neighbouring molecules can be considered as the input to the molecular device, while the resulting charge distribution can be considered as its output. We model the input as an external electric field, parallel to the *x* axis, hence to the main axis of the carbon chain (slightly tilted when the molecule is deposited on the Au(111) surface), and we control the electronic response of the molecule to this perturbation. In fact, the electric-field driven electron-transfer in mixed valence molecules has been experimentally demonstrated[18,20,33,58,59] and theoretically simulated in different MV systems.[11,21,28,60–63] Other aspects, out of the scope of this work, have to be considered for practical applications of mQCA cells in energy gain and power dissipation, state latching, tunnelling effects, clocked QCA, *etc.*[57,64,65]

Fig. 6 shows how the spin density on the effective redox sites changes with the applied electric field, *i.e.*, the response curve to a coulombic perturbation. We consider that the effective redox site contains the Ru ion plus the six closest carbon atoms of the polyynediyl chain, the spin density being greater on the chain part than in the Ru atom, as previously reported for parent dinuclear Ru mixed valence complexes bridged by polyynediyl linkers.[49] Note that the response curve is asymmetric, due to the presence of the counterion. In zero electric field, the unpaired electron (the hole) is localized on the effective redox site around Ru(1), placed in the positive part of the *x* axis in our internal coordinate system. In a simplified picture, this end side of the molecule can be considered as the positive pole (carrying the hole), while the opposite side around Ru(2) is the negative pole (with one excess electron). In the presence of a positive electric field along the *x* axis, the electronic distribution of the molecule is a bit more concentrated around the Ru(1) site, and the charge distribution is in fact stabilized by the applied field (Fig. 6). However, a negative electric field pushes the hole (the positive charge) to the opposite end of the molecule, changing the electronic distribution of the molecule. For an applied field larger than 0.002 a.u. (0.103 V $Å^{-1}$), we observe the electron transfer from the Ru(1) to Ru(2) effective site. The molecule switches the ground state under the effect of the external electric field (Fig. 6).

A further step should be the nuclear relaxation of the molecule, promoted by this new electronic distribution. The nuclear relaxation will act as a kind of self-trapping mecha-

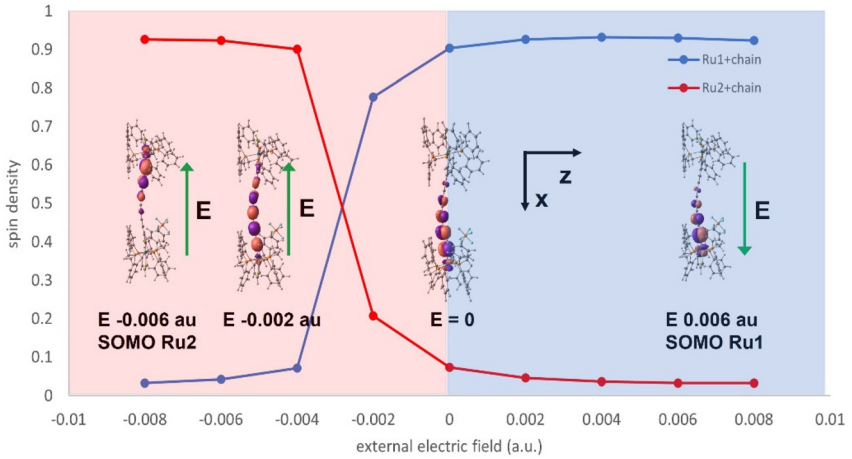

Fig. 6 Response curve of the **Ru2**$^{+}$ molecule under an applied electric field (in atomic units, 1 a.u. = 51.4 V Å^{-1}) along the long axis of the molecule. Blue (red) area corresponds to positive (negative) electric fields. The insets show the shape of the singly occupied orbital of the dominant configuration of the ground state CASSCF(7/4) wavefunction.

nism, enhancing the localization of the unpaired electron around the Ru(2) centre.

Additionally, we analyzed the electronic structure of the ground triplet state of a cell composed of two **Ru2**$^{+}$ molecules, as a model of a four-dot two-electron QCA cell. They are disposed in a similar orientation to that observed in the STM images of the deposited **Ru2** on Au(111). The intermolecular Ru–Ru distance is fixed to 14.949 Å, close to the intramolecular Ru–Ru distance of 17.753 Å (Fig. 7). The geometry employed is not optimized and similar conformations can be envisaged; thus these calculations should be considered just as a proof of concept. The CASSCF calculation of the lowest triplet states gives four roots close in energy, representing the four possible distributions of the unpaired electrons on the symmetric and antisymmetric combination of the $4d_{xz}$ and $4d_{xy}$ orbitals of Ru(1), with a relevant participation of the π_z and π_x orbitals, respectively, of the closest carbon atoms of the bridge chain, as observed for the single molecule. Fig. 7 presents one of the singly occupied orbitals of the dominant configuration of the ground triplet. It consists of the antisymmetric combination of the SOMO of the **Ru2**$^{+}$ molecule. The other singly occupied orbital of the triplet wavefunction is the corresponding symmetric combination. The molecules in the cell exhibit antipodal charge densities, compliant with the molecular QCA requirements.

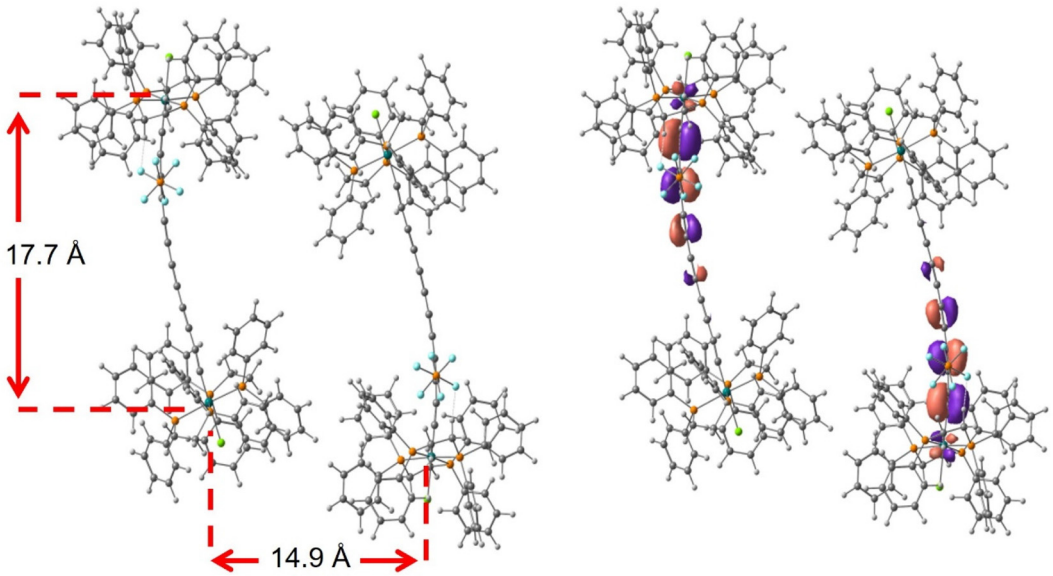

Fig. 7 A cell composed of two **Ru2**$^{+}$ molecules, in disposition like that observed in STM images. Singly occupied orbital of the ground triplet state, mainly localized on Ru(1) sites and the closest carbon atoms of the bridge chain.

4. Conclusions

The STM images of the *in situ* oxidized **Ru2** molecule deposited on Au(111) show two features of different contrasts (bright and dim), associated with the asymmetric charge distribution between the two end groups of the $\mathbf{Ru2}^{+}$ molecule.[31] Moreover, the $\mathbf{Ru2}^{+}$ complexes are organized on the surface forming rows by alternating polarization of neighbouring molecules similar to a QCA binary wire. We have explored by combining different state-of-the-art quantum chemistry approaches the deposition of the mixed-valence $\mathbf{Ru2}^{+}$ molecule on Au(111). Our calculations confirm the presence of two different end groups on the molecule, one of them close to the PF_6^- counterion, which corresponds to the Ru centre carrying the excess hole, *i.e.*, the extra positive charge of the molecule. The interaction with the substrate deforms the molecule and differentiates the two Ru centres. The analysis of the wavefunction of the doublet ground state corroborates the charge localization, and the unpaired electron is localized in the end group of the molecule close to the counterion. The redox site involves not only the Ru atom, but also the closest carbon atoms of the polyynediyl chain. The bright/dim features of the STM images could then be associated with these effective redox sites.

We have demonstrated that the polarization of the molecule can be switched by the action of the field induced by the neighbouring polarized driver cell. In fact, an electric field stronger than 0.002 a.u. (0.103 V $Å^{-1}$) is sufficient to promote the switching. Additionally, our results evidenced that a cell formed by two $\mathbf{Ru2}^{+}$ molecules present a charge distribution with two holes in the diagonal positions, in agreement with the alternating polarization observed along the molecular rows in the STM images.

In summary, this theoretical study corroborates the interpretation of the STM images proposed by Guo and Kandel,[31] and presents evidence of the role of the substrate in the localization of the charge and the potential of this system as a candidate for mQCA functionality.

Conflicts of interest

There are no conflicts of interest to declare.

Acknowledgements

The authors acknowledge the financial support through grant PGC2018-101689-B-I00 funded by MCIN/AEI/10.13039/501100011033 and by "ERDF A way of making Europe". C. J. C. thanks Dr Nadia Ben Amor for valuable discussions on the preliminary calculations of this system. The technical support of the Supercomputing Team of the Centro Informático Científico de Andalucía (CICA) and the access to the computational facilities of the "Centro de Servicios de Informática y Redes de Comunicaciones" (CSIRC, Universidad de Granada, Spain) and NLHPC(ECP-02) are also acknowledged.

References

1 J. V. Neumann and A. W. Burks, *Theory of Self-Reproducing Automata*, University of Illinois Press, 1966.
2 C. S. Lent, P. D. Tougaw, W. Porod and G. H. Bernstein, Quantum cellular automata, *Nanotechnology*, 1993, **4**, 49–57.
3 P. D. Tougaw and C. S. Lent, Logical devices implemented using quantum cellular automata, *J. Appl. Phys.*, 1994, **75**, 1818–1825.
4 A. O. Orlov, I. Amlani, G. H. Bernstein, C. S. Lent and G. L. Snider, Realization of a Functional Cell for Quantum-Dot Cellular Automata, *Science*, 1997, **277**, 928–930.
5 I. I. Amlani, A. O. Orlov, G. Toth, G. H. Bernstein, C. S. Lent and G. L. Snider, Digital logic gate using quantum-Dot cellular automata, *Science*, 1999, **284**, 289–291.
6 C. S. Lent, Bypassing the Transistor Paradigm, *Science*, 2000, **288**, 1597–1599.
7 N. Hush, Cool computing, *Nat. Mater.*, 2003, **2**, 134–135.
8 C. S. Lent, B. Isaksen and M. Lieberman, Molecular Quantum-Dot Cellular Automata, *J. Am. Chem. Soc.*, 2003, **125**, 1056–1063.
9 K. Hennessy and C. S. Lent, Clocking of molecular quantum-dot cellular automata, *J. Vac. Sci. Technol., B: Microelectron. Nanometer Struct. – Process., Meas., Phenom.*, 2001, **19**, 1752–1755.
10 X. Wang, L. Yu, V. S. S. Inakollu, X. Pan, J. Ma and H. Yu, Molecular Quantum Dot Cellular Automata Based on Diboryl Monoradical Anions, *J. Phys. Chem. C*, 2018, **122**, 2454–2460.
11 T. Groizard, S. Kahlal and J.-F. Halet, Zwitterionic Mixed-Valence Species for the Design of Neutral Clocked Molecular Quantum-Dot Cellular Automata, *Inorg. Chem.*, 2020, **59**, 15772–15779.
12 J. Ferrando-Soria, J. Vallejo, M. Castellano, J. Martínez-Lillo, E. Pardo, J. Cano, I. Castro, F. Lloret, R. Ruiz-García and M. Julve, Molecular magnetism, quo vadis? A historical perspective from a coordination chemist viewpoint, *Coord. Chem. Rev.*, 2017, **339**, 17–103.
13 J. A. Christie, R. P. Forrest, S. A. Corcelli, N. A. Wasio, R. C. Quardokus, R. Brown, S. A. Kandel, Y. Lu, C. S. Lent and K. W. Henderson, Synthesis of a Neutral Mixed-Valence Diferrocenyl Carborane for Molecular Quantum-Dot Cellular Automata Applications, *Angew. Chem., Int. Ed.*, 2015, **54**, 15448–15451.
14 Y. Lu and C. Lent, Self-doping of molecular quantum-dot cellular automata: mixed valence zwitterions, *Phys. Chem. Chem. Phys.*, 2011, **13**, 14928–14936.
15 B. Schneider, S. Demeshko, S. Neudeck, S. Dechert and F. Meyer, Mixed-Spin [2 × 2] Fe_4 Grid Complex Optimized for Quantum Cellular Automata, *Inorg. Chem.*, 2013, **52**, 13230–13237.
16 J. Jiao, G. J. Long, F. Grandjean, A. M. Beatty and T. P. Fehlner, Building Blocks for the Molecular Expression of Quantum Cellular Automata. Isolation and Characterization of a Covalently Bonded Square Array of

Two Ferrocenium and Two Ferrocene Complexes, *J. Am. Chem. Soc.*, 2003, **125**, 7522–7523.

17 J. Jiao, G. J. Long, L. Rebbouh, F. Grandjean, A. M. Beatty and T. P. Fehlner, Properties of a Mixed-Valence $(Fe^{II})_2(Fe^{III})_2$ Square Cell for Utilization in the Quantum Cellular Automata Paradigm for Molecular Electronics, *J. Am. Chem. Soc.*, 2005, **127**, 17819–17831.

18 Z. Li, A. M. Beatty and T. P. Fehlner, Molecular QCA Cells. 1. Structure and Functionalization of an Unsymmetrical Dinuclear Mixed-Valence Complex for Surface Binding, *Inorg. Chem.*, 2003, **42**, 5707–5714.

19 Z. Li and T. P. Fehlner, Molecular QCA Cells. 2. Characterization of an Unsymmetrical Dinuclear Mixed-Valence Complex Bound to a Au Surface by an Organic Linker, *Inorg. Chem.*, 2003, **42**, 5715–5721.

20 H. Qi, S. Sharma, Z. Li, G. L. Snider, A. O. Orlov, C. S. Lent and T. P. Fehlner, Molecular Quantum Cellular Automata Cells. Electric Field Driven Switching of a Silicon Surface Bound Array of Vertically Oriented Two-Dot Molecular Quantum Cellular Automata, *J. Am. Chem. Soc.*, 2003, **125**, 15250–15259.

21 V. Arima, M. Iurlo, L. Zoli, S. Kumar, M. Piacenza, F. Della Sala, F. Matino, G. Maruccio, R. Rinaldi, F. Paolucci, *et al.*, Toward quantum-dot cellular automata units: thiolated-carbazole linked bisferrocenes, *Nanoscale*, 2012, **4**, 813–823.

22 A. Palii, S. Aldoshin and B. Tsukerblat, Mixed-valence clusters: Prospects for single-molecule magnetoelectrics, *Coord. Chem. Rev.*, 2021, **426**, 213555.

23 T. Groizard, S. Kahlal and J.-F. Halet, Theoretical studies of mixed-valence organometallic species for potential utilization as quantum cellular automata, *J. Organomet. Chem.*, 2017, **844**, 35–42.

24 B. Tsukerblat, A. Palii, S. Zilberg, D. Korchagin, S. Aldoshin and J. M. Clemente-Juan, Vibronic recovering of functionality of quantum cellular automata based on bi-dimeric square cells with violated condition of strong Coulomb repulsion, *J. Chem. Phys.*, 2022, **157**, 074308.

25 A. Palii, A. Rybakov, S. Aldoshin and B. Tsukerblat, Semiclassical versus quantum-mechanical vibronic approach in the analysis of the functional characteristics of molecular quantum cellular automata, *Phys. Chem. Chem. Phys.*, 2019, **21**, 16751–16761.

26 B. Tsukerblat, A. Palii, J. M. Clemente-Juan and E. Coronado, Mixed-valence molecular four-dot unit for quantum cellular automata: Vibronic self-trapping and cell-cell response, *J. Chem. Phys.*, 2015, **143**, 134307.

27 A. Palii, S. Aldoshin and B. Tsukerblat, Towards the design of molecular cells for quantum cellular automata: critical reconsideration of the parameter regime for achieving functionality, *Dalton Trans.*, 2022, **51**, 286–302.

28 E. P. Blair, S. A. Corcelli and C. S. Lent, Electric-field-driven electron-transfer in mixed-valence molecules, *J. Chem. Phys.*, 2016, **145**, 014307.

29 Y. Lu and C. S. Lent, A metric for characterizing the bistability of molecular quantum-dot cellular automata, *Nanotechnology*, 2008, **19**, 155703.

30 N. A. Wasio, R. C. Quardokus, R. P. Forrest, S. A. Corcelli, Y. Lu, C. S. Lent, F. Justaud, C. Lapinte and S. A. Kandel, STM Imaging of Three-Metal-Center Molecules: Comparison of Experiment and Theory For Two Mixed-Valence Oxidation States, *J. Phys. Chem. C*, 2012, **116**, 25486–25492.

31 S. Guo and S. A. Kandel, Scanning Tunneling Microscopy of Mixed Valence Dinuclear Organometallic Cations and Counterions on Au(111), *J. Phys. Chem. Lett.*, 2010, **1**, 420–424.

32 S. Rigaut, J. Perruchon, L. Le Pichon, D. Touchard and P. H. Dixneuf, *J. Organomet. Chem.*, 2003, **670**, 37–44.

33 H. Qi, A. Gupta, B. C. Noll, G. L. Snider, Y. Lu, C. Lent and T. P. Fehlner, Dependence of Field Switched Ordered Arrays of Dinuclear Mixed-Valence Complexes on the Distance between the Redox Centers and the Size of the Counterions, *J. Am. Chem. Soc.*, 2005, **127**, 15218–15227.

34 B. Chaudret, G. Commenges and R. Poilblanc, Bis(diphenylphosphino)methane complexes of ruthenium(0) and ruthenium(II), *J. Chem. Soc., Dalton Trans.*, 1984, 1635–1639.

35 A. A. Adeniyi and P. A. Ajibade, Exploring the Ruthenium-Ligands Bond and Their Relative Properties at Different Computational Methods, *J. Chem.*, 2016, **2016**, 3672062.

36 C. Lee, W. Yang and R. G. Parr, Development of the Colle-Salvetti correlation-energy formula into a functional of the electron density, *Phys. Rev. B: Condens. Matter Mater. Phys.*, 1988, **37**, 785–789.

37 M. Renz, K. Theilacker, C. Lambert and M. Kaupp, A reliable quantum-chemical protocol for the characterization of organic mixed-valence compounds, *J. Am. Chem. Soc.*, 2009, **131**, 16292–16302.

38 M. Kaupp, M. Renz, M. Parthey, M. Stolte, F. Würthner and C. Lambert, Computational and spectroscopic studies of organic mixed-valence compounds: where is the charge?, *Phys. Chem. Chem. Phys.*, 2011, **13**, 16973–16986.

39 F. Neese, The ORCA program system, *Wiley Interdiscip. Rev.: Comput. Mol. Sci.*, 2012, **2**, 73–78.

40 C. Fourmental, S. Mondal, R. Banerjee, A. Bellec, Y. Garreau, A. Coati, C. Chacon, Y. Girard, J. Lagoute, S. Rousset, *et al.*, Importance of Epitaxial Strain at a Spin-Crossover Molecule–Metal Interface, *J. Phys. Chem. Lett.*, 2019, **10**, 4103–4109.

41 S. Gueddida and M. Alouani, Spin crossover in a single Fe $(phen)_2(NCS)_2$ molecule adsorbed onto metallic substrates: An ab initio calculation, *Phys. Rev. B: Condens. Matter Mater. Phys.*, 2013, **87**, 144413.

42 S. Gueddida, M. Gruber, T. Miyamachi, E. Beaurepaire, W. Wulfhekel and M. Alouani, Exchange Coupling of Spin-Crossover Molecules to Ferromagnetic Co Islands, *J. Phys. Chem. Lett.*, 2016, **7**, 900–904.

43 Y. Zhang, Surface effects on temperature-driven spin crossover in $Fe(phen)_2(NCS)_2$, *J. Chem. Phys.*, 2020, **153**, 134704.

44 Y. Zhang, $Fe(phen)_2(NCS)_2$ on Al(100): influence of AlN layer on spin crossover barrier, *Phys. Chem. Chem. Phys.*, 2021, **23**, 23758–23767.

45 S. Javaid, S. Lebègue, B. Detlefs, F. Ibrahim, F. Djeghloul, M. Bowen, S. Boukari, T. Miyamachi, J. Arabski, D. Spor, *et al.*, Chemisorption of manganese phthalocyanine on Cu (001) surface promoted by van der Waals interactions, *Phys. Rev. B: Condens. Matter Mater. Phys.*, 2013, **87**, 155418.

46 J. M. Soler, E. Artacho, J. D. Gale, A. García, J. Junquera, P. Ordejón and D. Sánchez-Portal, The SIESTA method forab initioorder-Nmaterials simulation, *J. Phys.: Condens. Matter*, 2002, **14**, 2745–2779.

47 T. Stuyver, J. Huang, D. Mallick, D. Danovich and S. Shaik, TITAN: A Code for Modeling and Generating Electric Fields-Features and Applications to Enzymatic Reactivity, *J. Comput. Chem.*, 2020, **41**, 74–82.

48 M. I. Bruce, B. G. Ellis, P. J. Low, B. W. Skelton and A. H. White, Syntheses, structures, and spectro-electrochemistry of {Cp*(PP)Ru}C≡CC≡C{Ru(PP)Cp*} (PP = dppm, dppe) and their mono- and dications, *Organometallics*, 2003, **22**, 3184–3198.

49 M. I. Bruce, K. Costuas, T. Davin, B. G. Ellis, J.-F. Halet, C. Lapinte, P. J. Low, M. E. Smith, B. W. Skelton, L. Toupet, *et al.*, Iron versus Ruthenium: Dramatic Changes in Electronic Structure Result from Replacement of One Fe by Ru in $[\{Cp^*(dppe)Fe\}\text{-}CC\text{-}CC\text{-}\{Fe(dppe)Cp^*\}]^{n+}$ (n = 0, 1, 2), *Organometallics*, 2005, **24**, 3864–3881.

50 Y. Tanaka and M. Akita, Organometallic radicals of iron and ruthenium: Similarities and dissimilarities of radical reactivity and charge delocalization, *Coord. Chem. Rev.*, 2019, **388**, 334–342.

51 N. S. Hush, Adiabatic Rate Processes at Electrodes. I. Energy–Charge Relationships, *J. Chem. Phys.*, 1958, **28**, 962–972.

52 N. S. Hush, Intervalence-Transfer Absorption. Part 2. Theoretical Considerations and Spectroscopic Data, *Prog. Inorg. Chem.*, 1967, 391–444.

53 N. S. Hush, Adiabatic theory of outer sphere electron-transfer reactions in solution, *Trans. Faraday Soc.*, 1961, **57**, 557–580.

54 N. S. Hush, Homogeneous and heterogeneous optical and thermal electron transfer, *Electrochim. Acta*, 1968, **13**, 1005–1023.

55 R. A. Marcus, On the Theory of Oxidation–Reduction Reactions Involving Electron Transfer. I, *J. Chem. Phys.*, 1956, **24**, 966–978.

56 R. A. Marcus, Theory of Electron-Transfer Reaction Rates of Solvated Electrons, *J. Chem. Phys.*, 1965, **43**, 3477–3489.

57 E. Rahimi and J. R. Reimers, Molecular quantum cellular automata cell design trade-offs: latching vs. power dissipation, *Phys. Chem. Chem. Phys.*, 2018, **20**, 17881–17888.

58 Y. Lu, R. Quardokus, C. S. Lent, F. Justaud, C. Lapinte and S. A. Kandel, Charge Localization in Isolated Mixed-Valence Complexes: An STM and Theoretical Study, *J. Am. Chem. Soc.*, 2010, **132**, 13519–13524.

59 A. Aviram and P. Roland, The Effect of Electric Fields on Double-Well-Potential Molecules, *Ann. N. Y. Acad. Sci.*, 1998, **852**, 339–348.

60 N. Liza, Y. Lu and E. P. Blair, Designing boron-cluster-centered zwitterionic Y-shaped clocked QCA molecules, *Nanotechnology*, 2022, **33**, 465201.

61 N. Liza, D. Murphey, P. Cong, D. W. Beggs, Y. Lu and E. P. Blair, Asymmetric, mixed-valence molecules for spectroscopic readout of quantum-dot cellular automata, *Nanotechnology*, 2022, **33**, 115201.

62 N. S. Hush, A. T. Wong, G. B. Bacskay and J. R. Reimers, Electron and energy transfer through bridged systems. 6. Molecular switches: the critical field in electric field activated bistable molecules, *J. Am. Chem. Soc.*, 1990, **112**, 4192–4197.

63 A. Farazdel, M. Dupuis, E. Clementi and A. Aviram, Electric-field induced intramolecular electron transfer in spiro .pi.-electron systems and their suitability as molecular electronic devices. A theoretical study, *J. Am. Chem. Soc.*, 1990, **112**, 4206–4214.

64 J. Timler and C. S. Lent, Power gain and dissipation in quantum-dot cellular automata, *J. Appl. Phys.*, 2002, **91**, 823–831.

65 P. Cong and E. P. Blair, Robust Electric-Field Input Circuits for Clocked Molecular Quantum-Dot Cellular Automata, *IEEE Trans. Nanotechnol.*, 2022, **21**, 424–433.

